Technical Report

Model-based Development Technology to Enhance the Performance of Steels for Automobiles

Takeshi KAWACHI* Yasuharu TANAKA
Takahiro AITO Masahiko ABE

Abstract

To maximize the performance of steel products and enhance the performance of automobiles, this report introduces Model-Based Development (MBD) technologies developed from the perspective of a steel manufacturer. These technologies include stiffness evaluation techniques that use numerical analysis to identify weaknesses in vehicle body stiffness, prediction techniques for material fracture that affect deformation modes during vehicle collisions, and factor analysis techniques that identify the causes of reduced shape fixation in parts produced by press forming. The report demonstrates how these technologies are utilized in the automobile development process and verifies their effectiveness.

1. Introduction

In recent years, automobiles have been required to satisfy increasingly diverse performance demands, including lightweight design combined with high crashworthiness, handling stability, noise and vibration (NV) performance, and superior fuel economy, while satisfying these requirements at a high level. Accordingly, automotive development involves adjusting various parameters—such as materials, sheet thickness, and structural geometry—to achieve an optimal balance among these requirements. In the medium to long term, the electrification of automobiles is expected to accelerate,[1] which will further complicate body design optimization. Specifically, as electric vehicles are equipped with heavy battery packs, increasing requirements for higher stiffness and structural durability pose significant challenges for body design optimization. In addition to these circumstances, there is a strong demand for shortening development cycles and reducing development costs. Consequently, the automotive industry has recently been accelerating the adoption of Model-Based Development (MBD) techniques.[2–5] MBD is a development methodology that integrates design, simulation, and verification primarily using Computer Aided Engineering (CAE) technology. Compared with the conventional trial-and-error process of iterative design and prototype verification, MBD enables more efficient and highly accurate design. Appropriate use of MBD techniques throughout the entire process from the initial planning stage to the final design can reduce physical verification steps, such as prototyping and experimental evaluation, thereby shortening development lead time and reducing costs.

As shown in **Fig. 1**, Nippon Steel Corporation has developed MBD technologies from a steel manufacturer's perspective to fully utilize the material properties of steel products and enhance automotive performance. These include:

- Stiffness evaluation technology,[6–8] which employs numerical analysis to identify weaknesses in vehicle body stiffness that influence driving stability and NV performance under operating conditions,
- Collision and fracture prediction technology,[9–14] which assesses resistance to deformation under collision conditions and predicts fracture behavior of materials and spot welds during impact events,
- Forming limit and dimensional accuracy prediction technology[15] for press forming of automotive components, and
- High-precision spot welding FEM analysis system,[16] which performs coupled analysis of electric, thermal, and stress fields while considering material phase transformations during spot welding of steel sheets,

and offer effective solutions to technical challenges in automotive development.

This paper presents analyses and examples of countermeasure using NSafe™-SV-espace, a strain-of-space-based analysis technology for stiffness evaluation designed to identify stiffness weaknesses. This approach enables efficient investigation of countermeasures to mitigate reductions in body stiffness resulting from the thinning

* Dr.Eng., Senior Researcher, Integrated Steel-Solution Research Lab.-I, Steel Research Laboratories
20-1 Shintomi, Futtsu City, Chiba Pref. 293-8511

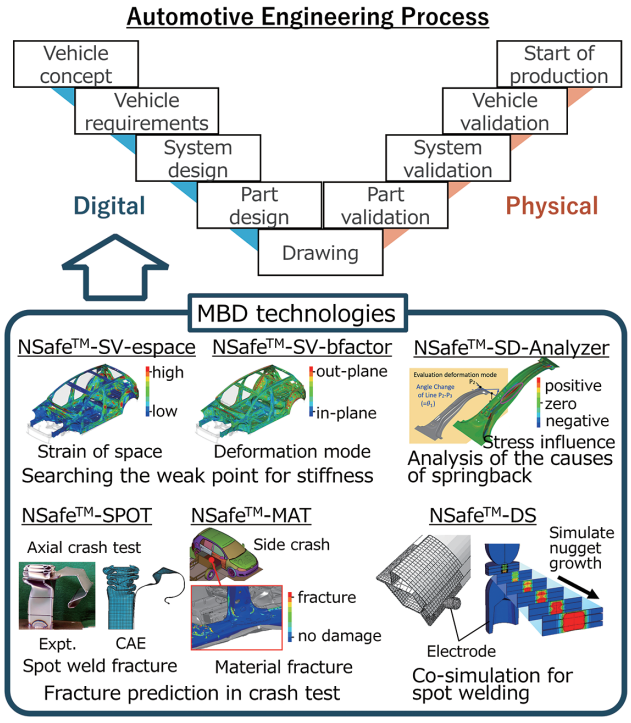

Fig. 1 Application of model-based development in automotive engineering processes

of steel sheets for weight reduction. Next, to support structural design that maximizes the performance of ultra-high-strength steel sheets,[17,18] whose application rate has been increasing to improve crashworthiness, a technology for predicting fracture initiation from punched edges using NSafe™-MAT is presented. This technology predicts steel sheet fracture behavior during collisions using CAE simulations. Finally, NSafe™-SD-Analyzer is introduced as a tool for addressing one of the challenges resulting from the increased application of high-strength steel—springback deformation of components after press forming, which represents a reduction in shape fixation. This tool analyzes the factors causing springback and supports efficient die modification and component design adjustments.

2. Stiffness Evaluation Technology

2.1 Challenges associated with thin-gauge steel in automotive structures

Steel has historically served as a fundamental material in automotive manufacturing. The adoption of ultra-high-strength steel, thin-gauge steel sheets has enabled improvements in crashworthiness and enhanced fuel and energy efficiency through vehicle weight reduction.[17] However, the use of thinner steel sheets may compromise body stiffness, potentially affecting handling stability and ride comfort.[19] Consequently, improving body stiffness has become a critical design objective, and numerous methods have been reported by automotive OEMs.[20,21] During vehicle development, stiffness and vibration analyses simulating load inputs encountered during driving are performed from the early stages to meet the stiffness targets established during product planning. In these analyses, input loads are transmitted through elements and nodes representing components and their connections (e.g., spot welds, bolts, adhesives), resulting in static or dynamic deformation of the entire vehicle model. Such deformation generates strain energy within each body component, inducing reaction forces that seek to restore the original geometry. At this stage, maximizing structural stiffness is equivalent to minimizing strain energy within the structure.[21] Increasing the thickness of components exhibiting high strain energy density or modifying their geometry to improve stiffness is widely recognized as an effective countermeasure. However, a limitation exists: regions with weak inter-component connections may form stiffness weak points, yet exhibit low strain energy, rendering them difficult to detect through strain energy density analysis. Therefore, the effectiveness of NSafe™-SV-espace is evaluated—a method that identifies stiffness weak points by analyzing relative displacement between components and derives structural countermeasures for these regions.

2.2 Method for identifying stiffness weak points based on relative displacement between components

Figure 2 illustrates the conceptual representation of relative displacement occurring between components. Although a multi-component structure exhibits overall displacement as a unified system, relative displacement arises from variations in inter-component connection strength and strain distribution within individual elements. The rate of change in relative displacement is defined as strain of space—a quantitative metric representing inter-component displacement—as expressed in the following equation.

$$\varepsilon_A = \frac{1}{n}\sum_{i=1}^{n}\left|\frac{L'_{Ai}-L_{Ai}}{L_{Ai}}\right|$$

This metric denotes the average rate of change in distance between an evaluation node and nodes located within the designated evaluation region. A lower strain of space reflects stronger inter-component linkage, indicating improved structural coupling. The evaluation region should be configured to correspond to the scale of the intended structural countermeasure.[6] **Figure 3** presents a comparison between strain energy density and strain of space under torsional loading in a closed-section structure comprising two hat components joined by a single backplate, with emphasis on the weak coupling region where the two hat components are adjacent. Strain energy density remains relatively low in these weak connections and is mainly used to visualize critical areas under the assumption of maintaining the existing structural configuration. Conversely, strain of

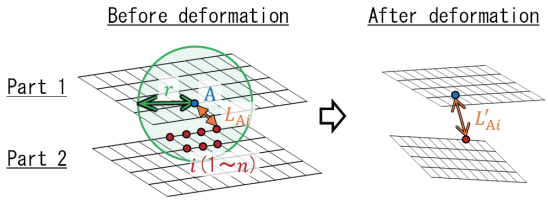

Fig. 2 Schematic image of relative displacement between parts

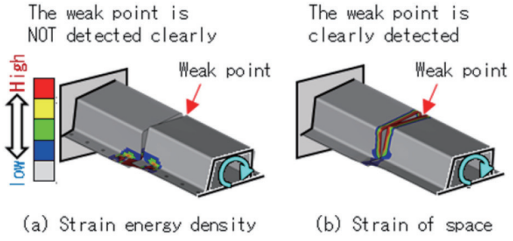

Fig. 3 Comparison of evaluation methods for weak point of bonding

space shows elevated values in these weak connections, allowing the identification of such regions even within complex assemblies such as body-in-white (vehicle bodies incorporating stiffening components) and supporting the visualization of areas requiring structural reinforcement.

2.3 Development of a method for deriving countermeasure structures for stiffness weak points

The method described in the previous section identifies stiffness weak points but does not provide specific structural countermeasure. Consequently, its capability to reduce the time and cost required to derive effective countermeasure structures remains limited. Therefore, a method was developed that employs strain of space to derive structural countermeasures aimed at improving stiffness. Multiple rigid beam elements are generated, originating from nodes exhibiting high strain of space. The endpoints of these elements are nodes located within a predefined range around the originating node, selected according to the highest rate of distance change relative to the originating node. Additionally, to prevent redundancy, each component is assigned only one endpoint, or the distance between endpoints is constrained to exceed a specified threshold. The stiffness improvement rate for each generated rigid beam element is evaluated, and elements demonstrating significant stiffness enhancement are extracted. By semi-automating this sequence of processes, structural countermeasures suitable for implementation can be derived with reduced lead time and cost.

2.4 Countermeasure study and effect verification using each evaluation method

This section investigates countermeasure structures and verifies their effectiveness using evaluation methods such as strain energy density and strain of space to improve stiffness. The analysis focuses on the platform's rear structure shown in **Fig. 4**, where the body's torsional stiffness is evaluated. Torsional stiffness is measured by constraining the rear damper mounting points and applying counter-parallel loads to the front dampers on both sides, thereby inducing torsion about the longitudinal axis.

First, a countermeasure study was conducted using the conventional strain energy density method. The strain energy density distribution during body torsional deformation, shown in **Fig. 5**, indicates high strain energy density in the rear side member (Part A), the connection between the rear cross member and Part A (Part B), and the stiffening component inside Part A (Part C). Since regions with high strain energy density can be regarded as critical for stiffness, an attempt was made to improve stiffness by increasing the sheet thickness of the above components. Specifically, the rear side member thickness was increased from 1.4 mm to 1.6 mm, Part B from 1.2 mm to 2.0 mm, and Part C from 1.25 mm to 2.0 mm. The resulting torsional stiffness improvement rate and mass increase were quantitatively evaluated.

Next, a study was performed using strain-of-space-based analysis. The strain of space distribution shown in **Fig. 6** evaluates and visualizes strain of space distribution at each node, focusing on components forming the body frame within a 100 mm evaluation radius. High strain of space was observed on the inner side of the rear side member. **Figure 7** presents the rigid beam elements with high stiffness improvement potential, derived through the structural derivation method targeting regions of insufficient stiffness introduced in the previous section. Reinforcing the connections between the rear side member's inner side (P_0), where strain of space is high,

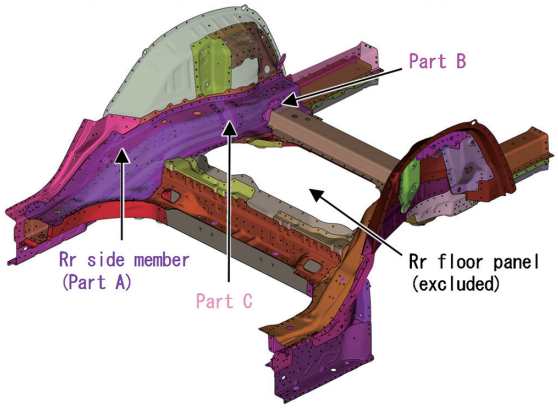

Fig. 4 Analysis area

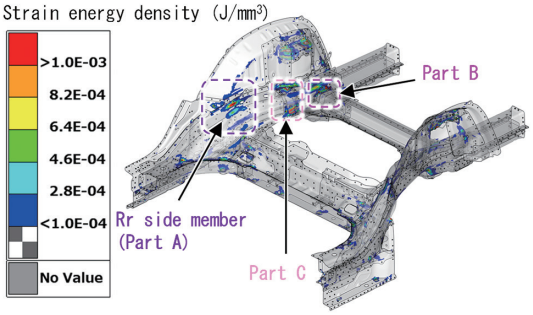

Fig. 5 Strain energy density distribution in body torsion

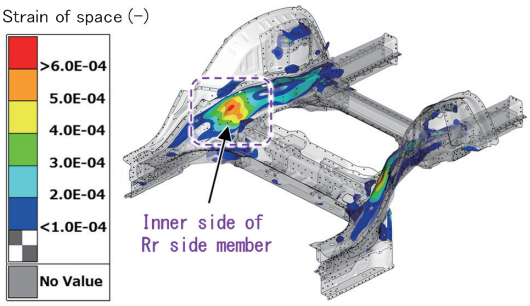

Fig. 6 Strain of space distribution in body torsion

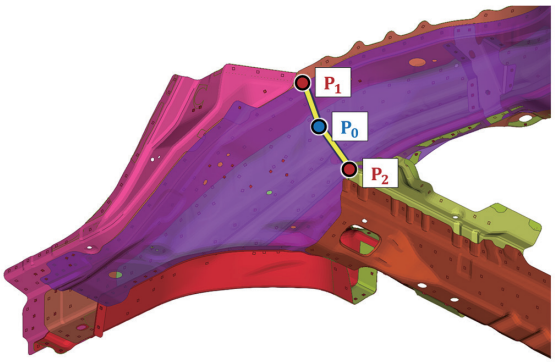

Fig. 7 Connections with high stiffness improvement

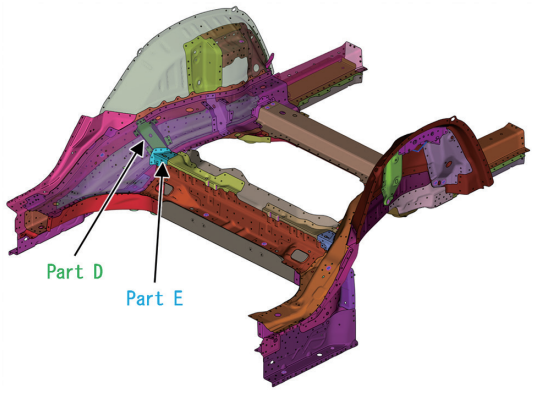

Fig. 8 Modified structure based on strain of space

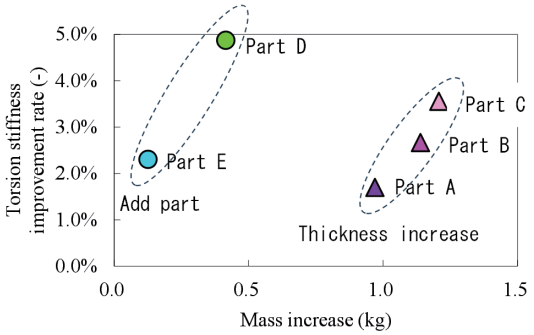

Fig. 9 Torsional stiffness improvement rate and mass increase for each modification

and points with large distance change rates relative to P_0—namely the rear side member's outer side (P_1) and the cross member at the front of the rear floor panel (P_2)—is anticipated to enhance torsional stiffness significantly. **Figure 8** shows the evaluation results for torsional stiffness improvement and mass increase achieved by adding a new component (Part D) inside the rear side member and a joint reinforcement (Part E) between the front cross member and the rear side member.

Figure 9 summarizes the torsional stiffness improvement rate and mass increase achieved by the proposed countermeasure structures. Compared to increasing the sheet thickness in components with high strain energy density, adding components based on strain of space resulted in superior mass efficiency for improving torsional stiffness. These findings confirm the effectiveness of NSafe™-SV-espace, a method for identifying stiffness weak points and deriving countermeasure structures by focusing on strain of space.

3. Collision Performance Prediction Technology

3.1 Challenges and countermeasures in crash performance due to ultra-high-strength steel adoption

The application ratio of ultra-high-strength steel in automotive bodies is increasing year by year.[17,18] In crash tests, if structural members do not deform in the intended mode, sufficient energy absorption may not be achieved. When ultra-high-strength steel is applied to body structural members, there is concern about material and spot weld fractures in areas such as the bumper and front side members during frontal impacts, and the center pillar and side sills during side impacts. Fracture can disrupt the intended deformation mode, making body design more difficult than before. A characteristic of material fracture in ultra-high-strength steel is bending fracture caused by localized buckling deformation in the crushed area. Additionally, when holes or notches are present in areas subjected to tensile forces due to intrusion of the colliding object into the vehicle body, edge fracture may occur starting from strain concentration at the material edges, potentially leading to a decrease in performance (e.g., crash reaction force).[22]

It is essential to predict these fracture phenomena in advance using FEM analysis and implement countermeasures. For this purpose, NSafe™-MAT has been developed, a material fracture prediction software that can be applied even with relatively coarse mesh sizes, assuming use in large-scale models such as full car models.[23,24] Until now, fracture prediction functions have been developed for in-plane deformation and bending deformation of steel sheets. This report introduces a newly developed edge fracture prediction function addressing stretch flange deformation at holes and notches, which is a concern with ultra-high-strength steel.

One of the key material properties of steel sheets is local ductility, which accounts for damage caused by edge shearing, and is commonly evaluated using the hole expansion ratio. However, the hole expansion test involves axisymmetric deformation, where strain is scarcely distributed circumferentially before fracture occurs. In contrast, during actual crash deformation of structural components, various strain gradients arise due to notched geometries in addition to the damage introduced during punching. It is known that the fracture limit changes under the influence of these strain gradients. Therefore, by adding the hole expansion ratio as a new indicator defining material properties, we have constructed a new edge fracture prediction function capable of predicting the locally occurring strain gradient at the edge region for any element size while considering the influence of punching damage and responding to the sequentially changing strain gradient during deformation.

3.2 Development of edge fracture prediction function

To establish edge fracture criteria, a one-sided notched tensile test method was developed. This method allows varying the strain gradient from the notch root during tensile testing by using specimens with Type I, II, and III notches, as shown in **Fig. 10**. Furthermore, to incorporate the effects of punching damage into fracture

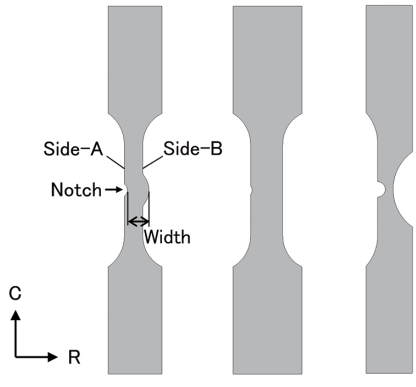

	Type I	Type II	Type III
Side-A notch depth	2 mm	1 mm	5 mm
Width at notch root	14 mm	20 mm	5 mm
Side-B shape	R15 Convex	Straight	R30 Concave

Fig. 10 Developed one-sided notched tensile test specimen shape

prediction, specimens were cut such that a φ10 mm punched hole (11% sheet thickness clearance), identical to that used in hole-expansion tests, served as the notch. As shown in **Fig. 11**, cracks initiated at the point of maximum stress for Types I and II. In contrast, Type III exhibited necking at the notch root before crack initiation. In this case, the necking was considered a defect, and the point of maximum stress attainment was defined as the fracture initiation point.

Figure 12 shows the maximum principal strain distribution at the fracture initiation timing and the principal strain distributions in the radial and circumferential directions from the notch root. For Type I, elements with high maximum principal strain are aligned circumferentially around the notch root. This indicates a small circumferential strain gradient between the notch root and adjacent elements, while a high radial strain gradient exists. In contrast, Type III has elements with high maximum principal strain aligned in the radial direction at the notch root. This indicates a small radial strain gradient between the notch root and adjacent elements, while a high circumferential strain gradient exists. Type II exhibits an intermediate strain gradient. By conducting these one-sided notched tensile tests on various materials with different hole expansion rates, the relationship between hole expansion rate, strain gradient, and ultimate strain at fracture was clarified. Furthermore, by identifying the correlation with the element size used in FEM analysis using a new metric, an edge fracture prediction function applicable to any element size was established.

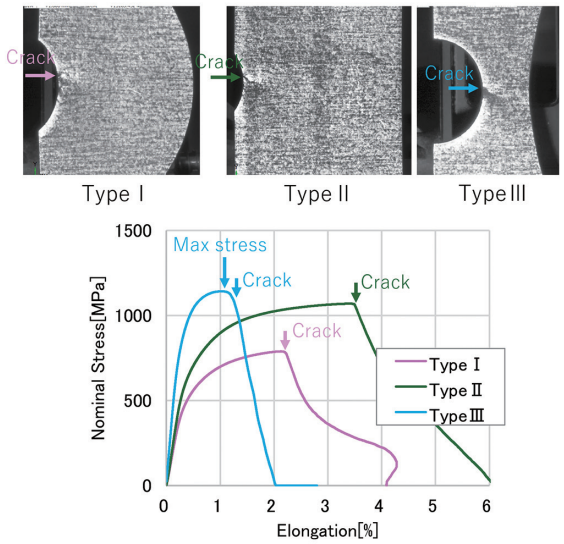

Fig. 11 Developed one-sided notched tensile test result (Gauge length 50 mm)

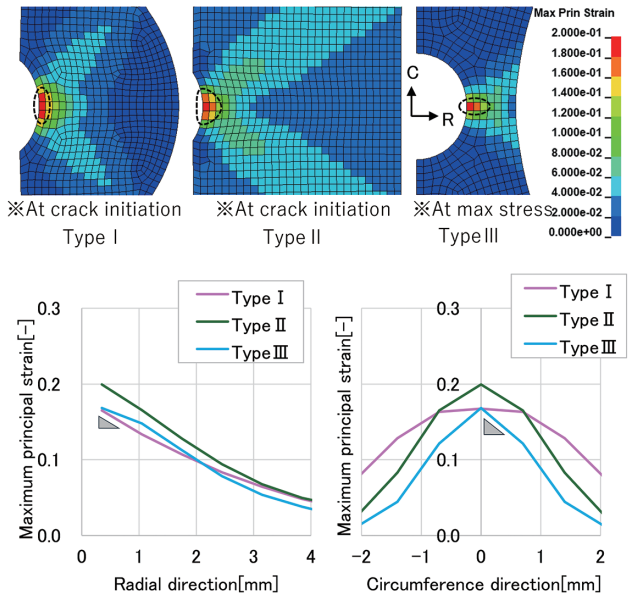

Fig. 12 Maximum principal strain distribution at fracture occurrence by FEM analysis of one-sided notched tensile test

3.3 Accuracy verification of edge fracture prediction function

Figure 13(a) shows the fracture elongation (gauge length 10 mm) for Type I, II, and III one-sided notched tensile tests performed on three steel grades (Material A, B, and C) with different hole expansion rates and n values. For Type I, higher hole expansion rates tended to result in higher fracture elongation, while for Type III, higher n values tended to result in higher fracture elongation. This indicates that the steel sheet property contributing to improved fracture elongation (hole expansion rate or n value) varies depending on the state of the strain gradient.

Next, Figs. 13(b), (c), and (d) show the results of predicting the fracture elongation obtained from the single-notch tensile tests for each steel grade using the developed NSafe™-MAT edge fracture prediction function. For comparison, when using the stress FLD[14] corresponding to the conventional in-plane tensile function of NSafe™-MAT, the timing of fracture detection was significantly delayed, particularly because it does not consider the edge condition.

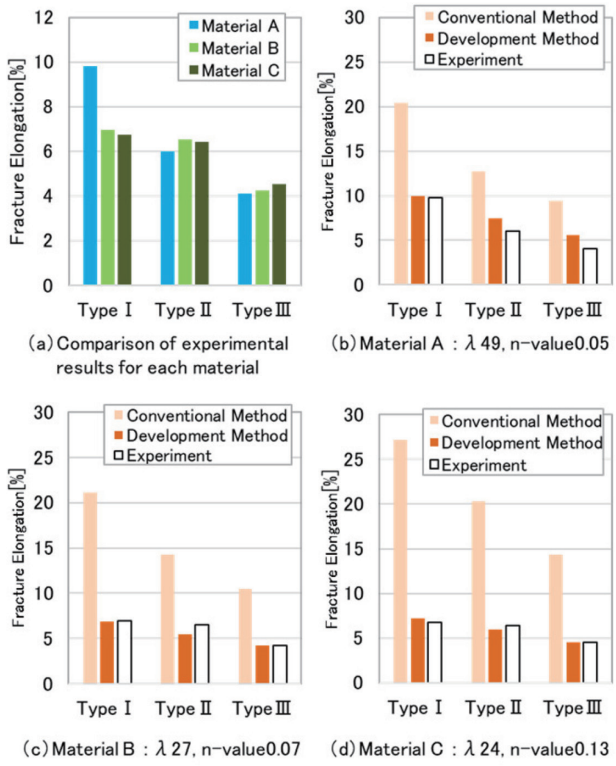

Fig. 13 One-side notched tensile test results and fracture elongation (gauge length 10 mm) prediction results by NSafe™-MAT

In contrast, the developed edge fracture prediction function was confirmed to accurately predict fracture elongation for all test specimen types (strain gradient states) made from steel grades with different sheet characteristics. This was achieved by varying the criteria based on the strain gradient state at the notch root during deformation, while considering the influence of the input hole expansion ratio.

Furthermore, to verify fracture prediction accuracy under conditions closer to actual automotive components, a compression bending test using a hat member was conducted to simulate a front side member front impact test.[25] The hat member measured 100 mm wide × 40 mm high × 300 mm long and used 980 MPa-grade steel sheet (1.6 mm thick, VDA bend angle 66°, hole expansion ratio 28%). A φ15 mm punched hole was made at the center position in the vertical wall height direction, 190 mm from the top edge of the hat member. The hat section and backplate, made of the same steel grade and thickness, were spot-welded at 25 mm intervals along the flange. Additionally, a trigger inducing transverse buckling deformation was incorporated 180 mm from the top edge of the hat member.

Figure 14(a) shows high-speed camera images from a drop impact test using a flat impactor (weight 751 kg, velocity 23 km/h). It was confirmed that edge fracture initiated from the punched hole edge at a 60 mm stroke, immediately after the start of lateral buckling deformation following crushing deformation at the top of the hat member. An FEM model reproducing these test conditions was created. Predictions using NSafe™-MAT confirmed accurate forecasting of bending fracture at the upper end's crushed region and, using the newly developed edge fracture prediction function, also accurately predicted fracture originating from the punched hole edge at a 69 mm stroke.

By incorporating the previously challenging effects of punched hole damage and strain gradient into fracture prediction, a new high-accuracy edge fracture prediction function was developed. This enables integrated material fracture prediction covering nearly all fracture modes possible in automotive components when combined with NSafe™-MAT's existing fracture prediction functions for in-plane deformation and out-of-plane deformation (bending deformation).

Furthermore, the edge fracture prediction function can evaluate whether fracture occurs in automotive components during collision analysis by using hole expansion rate as input. This allows the required hole expansion rate to achieve the desired collision performance to be calculated in reverse. Consequently, for example, in the early stages of material development, the necessary hole expansion rate value for the final automotive component product can be determined. This enables efficient material development with clear development goals and minimizes rework.

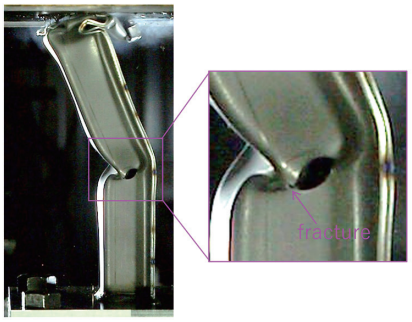

(a)Fracture from the edge of the punched hole at 60 mm stroke (High-speed camera image from experiment)

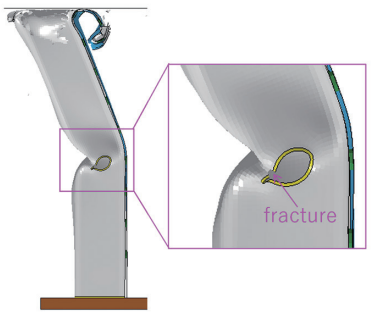

(b)Fracture from the edge of the punched hole at 69 mm stroke (NSafe™-MAT prediction)

Fig. 14 Prediction results of fracture from hole edge in compression bending drop weight test for frontal collision

4. Springback Analysis Technology

4.1 Challenges and countermeasures in press forming owing to increased strength of steel sheet

Increased material strength and the integration of large-scale body parts lead to challenges associated with production technology, such as difficulty in suppressing cracks and wrinkles owing to reduced formability, increased die-finishing lead times, and higher costs owing to greater springback. To address the issue of reduced formability, Nippon Steel has proposed and developed the NSafe™-FORM series[26, 27] press-forming method, in which shear deformation (a deformation mode with high yield strain in steel sheets) is used, enabling the production of various parts using ultra-high-strength steel.

However, for large parts made of ultra-high-strength steel sheets, springback often exceeds 10–20 mm, making through die design adjustments difficult to address. Effectively suppressing springback deformation by reducing the residual stress after press forming that causes springback deformation ("deformation-causing stress") through changes to part design or modifications to intermediate forming shapes is essential to ensure dimensional accuracy for such parts. Therefore, analyzing the deformation-causing stresses is crucial. Nippon Steel has developed the automated analysis system "NSafe™-SD-Analyzer (Springback Deformation Analyzer)," which enables rapid and detailed analysis based on the FEM springback analysis. The following section describes the analytical method for deformation-causing stresses and the results of analysis of these stresses using the NSafe™-SD-Analyzer.

4.2 Analytical method for springback deformation-causing stresses and automated analysis system

The fundamental analytical method for stress induced by springback deformation is as follows: Springback analysis is an elastic deformation analysis performed under conditions in which the constraints imposed by the die, represented by an FEM model obtained from the press-forming analysis that captures the shapes and stresses of the press panel at the bottom dead center during forming, are removed. A virtual condition model (stress-modified model) was created for the springback analysis model (base model) by varying the stress in a specific region of the press panel. An elastic deformation analysis was then performed on this model. By comparing the deformation of the base model with that of the stress-modified model, the sensitivity of the amount of springback deformation to the stress modification in the relevant region (stress influence) was determined. Furthermore, identifying regions with a high stress influence

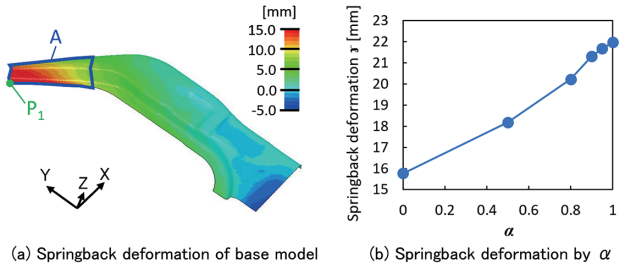

Fig. 15 Springback deformation of the base model and the effect of α

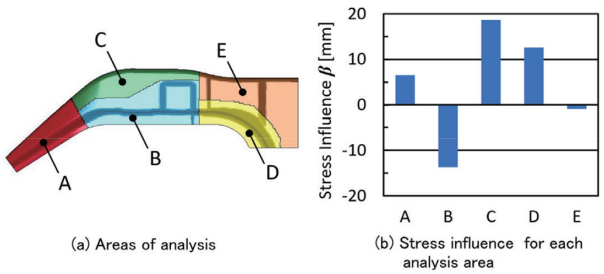

Fig. 16 Analysis area and stress influence

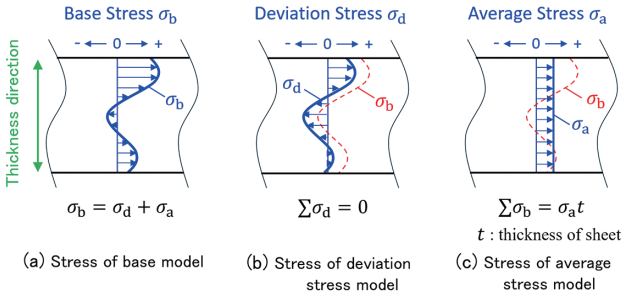

Fig. 17 Deviation stress and average stress

was possible by calculating and comparing the stress influence across multiple regions of the press panel. Examining the stresses in the identified regions of the base model enables the identification of the deformation-causing stress.

For example, for the part exhibiting springback deformation, as shown in **Fig. 15**(a), the base model is used, and a stress-modified model is created by modifying the stress in the region A shown in the figure by multiplying it by the coefficient α. The deformation-causing stresses can be identified by comparing the results of the analysis of this stress-modified model with those of the base model. Figure 15(b) shows the springback deformation amount γ obtained by varying α using the z-direction displacement at point P_1 (the point of maximum displacement) as the deformation mode. Because γ and α do not exhibit a perfectly linear relationship, various definitions of stress influence can be considered. For example, the stress influence β for the region A is calculated on the basis of the difference $\Delta\gamma$ between γ for the base model (i.e., $\alpha=1.0$) and γ for $\alpha=0.9$ while accounting for the proportion of stress change:

$$\beta=\frac{\Delta\gamma}{1-\alpha}=\frac{z_b-z_c}{1-\alpha}=\frac{21.97-21.32}{1-0.9}=6.5 \quad [\text{mm}]$$

where z_b and z_c represent γ for the base model and $\alpha=0.9$, respectively.

Furthermore, when the base model, as shown in Fig. 15(a), is divided into five regions, as shown in **Fig. 16**(a), and the stress influence for each region is similarly calculated, the resulting graph shown in Fig. 16(b) enables the assessment of the stress influence across the entire part.

However, the results of the analysis, as shown in Fig. 16, exhibit overlapping deformation modes, and the coarse division of the analysis regions makes the identification of the detailed deformation-causing stresses difficult. Springback deformation in actual parts involves multiple overlapping deformation modes, such as torsion, camber, wall buckling, and gap opening, necessitating an analysis for each deformation mode. In particular, the deformation caused by the deviation and average stress components exhibit different deformation modes, as shown in **Fig. 17**. Therefore, analyzing them separately facilitates the identification of the stresses responsible for deformation. Furthermore, the analysis domain must be refined to a level that corresponds to the stress distribution.

Manually performing such a detailed analysis is highly labor-intensive and impractical. Therefore, we developed an automated analysis system (NSafe™-SD-Analyzer) to perform detailed analysis.

NSafe™-SD-Analyzer first edits the base stress model to create a model that contains only deviation stress components (deviation stress base model) and a model containing only average stress components (average stress base model). Subsequently, it automatically divides the entire part into regions of specified sizes. For each region, a stress-modified model is created, the analysis is executed, the analysis results are read, and the stress influence for both the deviation and average stress base models is determined. Furthermore, the distribution of the stress influence is displayed as contours on the part geometry. Moreover, the springback deformation being evaluated can include not only node displacement but also various deformation modes, such as the distance between two points, twist, warpage, and angular change. The parallel computation of multiple stress-modified models is possible when the analysis is executed. Although a commercially available general-purpose solver can be used as the analysis solver, it also features a dedicated solver with a proprietary algorithm that accelerates calculations.

The following section describes the detailed analysis results obtained using NSafe™-SD-Analyzer.

4.3 Analysis model and method

The analysis model was the center pillar made of ultra-high-strength steel, as shown in **Fig. 18**; the model was formed using the "in-plane-shear draw-bending (NSafe™-FORM-LT)" method.[27] Based on the shape and stress data at the bottom dead center obtained from the forming analysis using a general-purpose dynamic explicit solver, a base model, a deviation stress base model, and an average stress base model were created. **Figures 19**(a), (b), and (c) show the results of springback analysis for each model. Further-

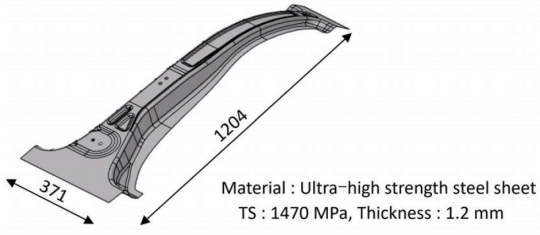

Fig. 18 Analysis model

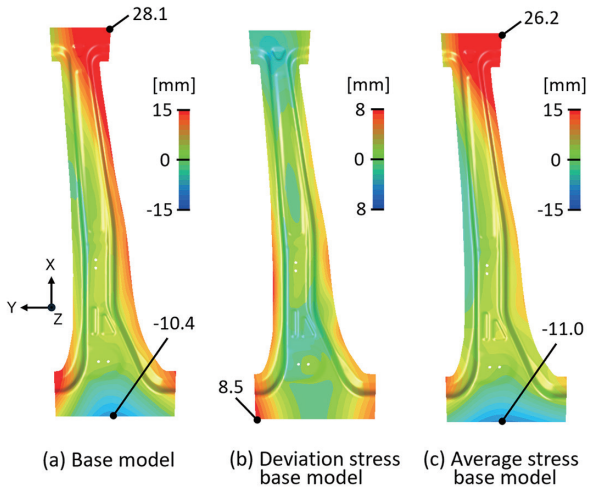

Fig. 19 Springback simulation results (z-direction displacement)

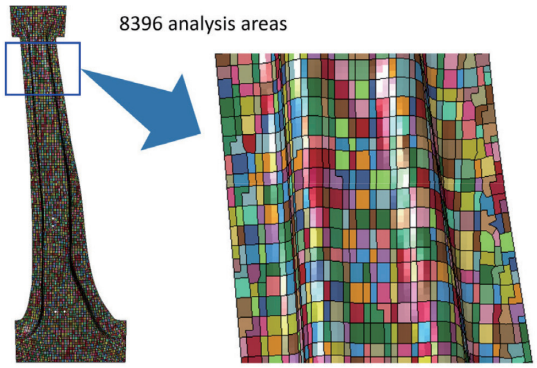

Fig. 20 Analysis area segmentation

more, the part was divided into 8396 small regions, each approximately 2–4 mm in size, as shown in **Fig. 20**. For both the deviation and average stress base models, stress-modified models for each region were created using $\alpha=0.9$, and the stress influences for all regions were calculated. Note that the processes after the creation of the base model were performed automatically.

4.4 Results of analysis of stress influence

As representative examples of the results of analysis of stress influence, **Fig. 21** shows the results of analysis of two deformation modes of springback: (1) twisting of the upper part and (2) deflection of the lower end, both of which are caused by the average stress, as shown in Fig. 19(c). The evaluation values for each deformation mode, as shown in the figure, are defined as the angle change of line P_2–P_3 (Mode 1) and the angle change of angle P_4–P_5–P_6 (Mode 2). The red areas in the stress-influence contour diagram indicate the regions where the deformation-causing stresses originate. Although multiple areas with high-influence stress were found, the primary deformation-causing stress regions were identified as section F, as shown in Fig. 21(a), for Mode 1 and section G, as shown in Fig. 21(b), for Mode 2.

This analysis automatically created 16792 stress-modified models, executed the analysis, read the results, and calculated the stress influence for both deviation and average stress base models. The total computation time was 11 h 16 min using 48-core parallel processing with 48 jobs. Because the computation time scales proportionally with the number of domains, reducing the analysis resolution or limiting the analyzed domains can decrease the computational load.

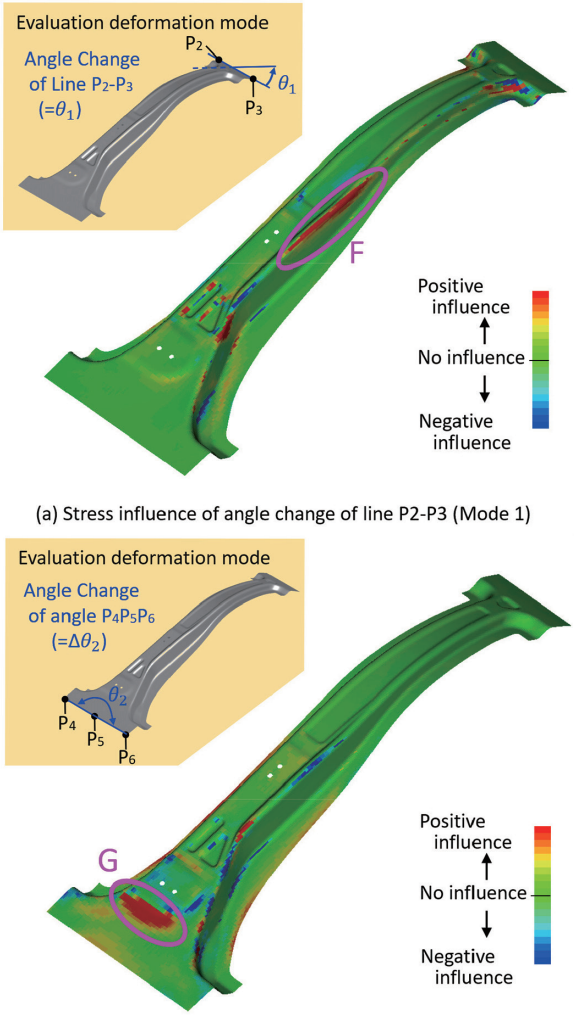

Fig. 21 Stress influence analysis results (Average stress base model)

4.5 Verification of results of analysis

From the stress influence contour maps of the analysis results, four regions corresponding to the deviation stress, with a total area ratio of 14.5% relative to the part, and fifteen regions corresponding to the average stress, with a total area ratio of 22.6% relative to the part, were identified as springback deformation-causing stress regions. To verify the results of analysis, we performed a springback analysis on a model in which the identified deformation-causing stresses were removed from the base model. The results are shown in **Fig. 22**. Compared with the base model shown in Fig. 19(a), the maximum springback deformation was significantly reduced from 28.1 to 4.4 mm, confirming the validity of the analysis.

5. Conclusion

This paper has presented automotive development support technologies based on Model-Based Development (MBD) developed by

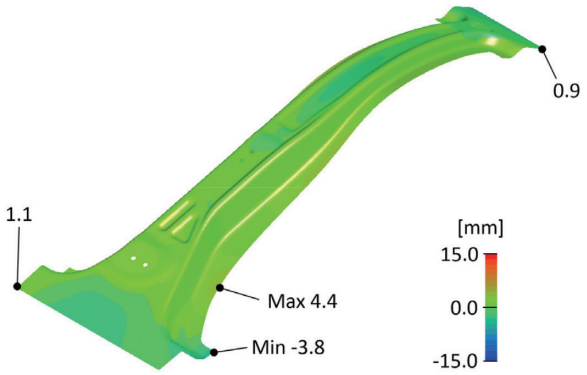

Fig. 22 Springback deformation after removal of dominant causal stress

Nippon Steel. For stiffness evaluation technology, NSafe™-SV-espace was demonstrated to identify weaknesses in vehicle body stiffness, thereby enabling efficient stiffness improvement. For crashworthiness prediction technology, NSafe™-MAT was introduced as a technique for predicting material fracture at punch edges, allowing pre-collision assessment of material fracture. For springback analysis, NSafe™-SD-Analyzer was demonstrated to identify the cause stresses of springback deformation after press forming, supporting efficient die modifications and component design adjustments. These technologies have provided effective solutions to various technical challenges in automotive development, contributing to streamlined processes, improved product quality, and cost reduction. Future work will include further technological development and expanded application of Nippon Steel proprietary MBD technologies to support the sustainable growth of the automotive industry.

References

1) Automobile Division, Manufacturing Industries Bureau, Ministry of Economy, Trade and Industry: The 4th Battery Industry Strategy Promotion Conference. Tokyo, 2025-3, Ministry of Economy, Trade and Industry
2) Ogata, E.: The 49th Joint Automatic Control Conference. 49 (19), 27 (2006)
3) Fujikawa, S.: Mazda Technical Review. (31), 44 (2013)
4) Wakiya, S. et al.: Journal of Japanese Society for Engineering Education. 66 (1), 80 (2018)
5) Antoku, M.: Nissan Technical Review. (89), 1 (2023)
6) Tsunemi, Y. et al.: Transactions of Society of Automotive Engineers of Japan. 51 (5), 789 (2020)
7) Kawachi, T. et al.: Transactions of Society of Automotive Engineers of Japan. 50 (5), 794 (2020)
8) Kawachi, T. et al.: Transactions of Society of Automotive Engineers of Japan. 53 (5), 799 (2022)
9) Yoshida, H. et al.: 2004 JSAE Annual Congress Proceedings (Spring). (8-04), 1 (2004)
10) Yoshida, H. et al.: 2005 JSAE Annual Congress Proceedings (Spring). (49-05), 9 (2005)
11) Aito, T. et al.: Nippon Seitetsu Giho. (409), 120 (2017)
12) Yonemura, S. et al.: Tetsu-to-Hagané. 93 (4), 317 (2007)
13) Uenishi, A. et al.: Shinnittetsu Giho. (393), 32 (2012)
14) Aito, T. et al.: Nippon Seitetsu Giho. (412), 86 (2019)
15) Yoshida, T. et al.: Shinnittetsu Giho. (392), 65 (2012)
16) Ueda, H. et al.: Shinnittetsu Sumikin Giho. (409), 108 (2017)
17) Takahashi, M.: Tetsu-to-Hagané. 100 (1), 82 (2014)
18) Japan Sheet Metal Forming Research Group: Puresu seikei nan'i handobukku [Press Forming Difficulty Handbook] 4th Edition. Tokyo, Japan Sheet Metal Forming Research Group, 2017, p.10
19) Matschinsky, W.: Road Vehicle Suspension. 1st ed. London, Professional Engineering Publishing Limited, 2000, 359p
20) Satomura, A. et al.: Transactions of the Japan Society of Mechanical Engineers. 91 (941), 1 (2025)
21) Wada, N. et al.: Transactions of Society of Automotive Engineers of Japan. 55 (1), 160 (2024)
22) Sato, K. et al.: 2013 JSAE Annual Congress Proceedings (Spring). (38-13), 1 (2013)
23) Yonemura, S. et al.: 2014 JSAE Annual Congress Proceedings (Spring). (46-14), 1 (2014)
24) Aito, T. et al.: Nippon Seitetsu Giho. (412), 86 (2019)
25) Aito, T. et al.: 2025 JSAE Annual Congress Proceedings (Spring). 2025 Spring, 107 (2025)
26) Tanaka, Y. et al.: Bulletin of the Japan Society for Technology of Plasticity. 6 (72), 725 (2023)
27) Tanaka, Y. et al.: Journal of the Japan Society for Technology of Plasticity. 60 (705), 283 (2019)

Takeshi KAWACHI
Dr.Eng., Senior Researcher
Integrated Steel-Solution Research Lab.-I
Steel Research Laboratories
20-1 Shintomi, Futtsu City, Chiba Pref. 293-8511

Takahiro AITO
Senior Researcher
Integrated Steel-Solution Research Lab.-I
Steel Research Laboratories

Yasuharu TANAKA
Dr.Eng., Chief Manager
Quality Management Div.
Nagoya Works

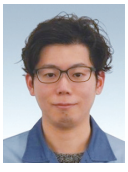

Masahiko ABE
Researcher
Integrated Steel-Solution Research Lab.-I
Steel Research Laboratories